

and a low-velocity region below the deep discontinuity were checked in FD wave form modeling. Processed data and FD synthetics obtained assuming a sharp increase in *P*-wave (and *S*-wave) velocity (6.0 to 6.8 km/s) and a sharp velocity decrease (6.0 to 2.7 km/s) at the 10-km discontinuity (Fig. 3) indicate that a velocity decrease as strong as that assumed is needed to generate large-amplitude *P*-to-*S* converted phases. Synthetics produced by this model reproduce the amplitude ratios of *PS* phases and other secondary energetic arrivals that interfere with them in the analyzed distance and time windows.

The occurrence of such mid-crustal high- to low-velocity discontinuities at depths of 10 to 20 km has been observed in several volcanic areas (19), where it is considered an indicator of large magmatic reservoirs. From our modeling, *P*-wave velocity in the low-velocity zone is lower than 2.5 to 3 km/s, which is consistent with the occurrence of magmatic melt within a high-permeability host rock. Fluid inclusions in Mount Vesuvius clinopyroxenes have been trapped at pressure corresponding to depths between 4 and 10 km. Seismic activity appears to be shallower than 6 to 8 km, indicating that the brittle-ductile transition zone is deeper. These data suggest that a melting zone can exist at a depth of 9 to 11 km, as inferred from the analysis of LALA phase.

REFERENCES AND NOTES

1. V. Arnò *et al.*, in *Somma-Vesuvius*, R. Santacroce, Ed. (Quaderni de La Ricerca Scientifica, Rome, 1987), pp. 53–103.
2. F. Barberi *et al.*, *Bull. Volcanol.* **44**, 295 (1981); L. Civetta, R. Galati, R. Santacroce, *ibid.* **53**, 517 (1991).
3. H. E. Belkin and B. De Vivo, *J. Volcanol. Geotherm. Res.* **58**, 89 (1993).
4. H. Sigurdsson, S. Carey, W. Cornell, T. Pescatore, *Natl. Geogr. Res.* **1**, 332 (1985).
5. P. Papale and F. Dobran, *J. Volcanol. Geotherm. Res.* **58**, 101 (1993).
6. P. Gasparini, M. S. M. Mantovani, R. Scandone, *Bull. Volcanol.* **44**, 317 (1981).
7. R. Santacroce, A. Bertagnini, L. Civetta, P. Landi, A. Sbrana, *J. Petrol.* **34**, 383 (1993); H. E. Belkin, C. J. Kilburn, B. De Vivo, *J. Volcanol. Geotherm. Res.* **58**, 273 (1993).
8. I. Finetti and C. Morelli, *Boll. Geofis. Teor. Appl.* **16**, 175 (1974).
9. C. Principe, M. Rosi, R. Santacroce, A. Sbrana, in *Somma-Vesuvius*, R. Santacroce, Ed. (Quaderni de La Ricerca Scientifica, Rome, 1987), pp. 11–52.
10. E. Cassano and P. La Torre, *ibid.*, pp. 175–196.
11. F. Ferrucci *et al.*, *Geophys. Res. Lett.* **16**, 1317 (1989).
12. The seismic stations (60 of the 82 were three-component digital recorders) deployed along the profile were spaced 250 m apart in the center of the profile (as far as 5 km northwest and southeast of the crater) and 500 m apart at the outer parts. Shot S1 was located on the carbonates of the Sorrento Peninsula, shot S2 was on the southeast slope of the volcano near the Trecase well, and shot S3 was on the south edge of the Mount Somma caldera rim.
13. Mount Vesuvius is presently affected by regular mi-

croseismicity (local magnitude $M_L < 3$) shallower than 5 to 6 km and concentrated beneath Gran Cono, as monitored by the permanent seismic network of Osservatorio Vesuviano. The data from shots S2 and S3 were integrated with arrival times from a selected set of 40 well-located microearthquakes, which provide additional constraints on the deeper part of the volcano edifice. The local earthquakes were preliminarily located in a structure that approximated the 2D initial model used for the tomographic inversion.

14. Methods for travel-time inversion and delay-time tomography were applied to direct *P*-wave arrival times from the seismic records of shots S2 and S3 at the stations located along the volcano slope. We estimated preliminary 1D velocity profiles for the shallow part of the volcano by using a revised version of the tau-*p* inversion method (20, 21). The 2D shallow structure of Somma-Vesuvius has been determined with a tomographic method in which the propagating medium is described by continuous functions interpolating linearly the velocities assigned to nonregular grid points (21). The ray paths were approximated by an arc of circles, and the solution was obtained by iterative, damped least squares. Space resolution was inferred from ad hoc tests using synthetic data from spike anomalies centered at different positions within the investigated section (21). Resolution is the highest (1.0 km laterally and 0.5 km vertically) at the center of the profile down to a depth of about 4 km and deteriorates laterally and downward.
15. J. Virieux, V. Farra, R. Madariaga, *J. Geophys. Res.* **93**, 6585 (1988); J. Virieux, *ibid.* **96**, 579 (1991).
16. A. Bernasconi, P. Bruni, L. Gorla, C. Principe, A. Sbrana, *Rend. Soc. Geol. Ital.* **4**, 237 (1981).
17. The arrival times of the LALA phase have been modeled by a trial and error approach with the use of a ray-tracing method for a laterally heterogeneous medium (22). A *P*-wave velocity model obtained by tomography was used in the layer above the V-L interface. A linear increase of *P*-wave velocity with depth

with a gradient of 0.05 s⁻¹ was assumed below the V-L interface. The V_P/V_S ratio has been assumed to be homogeneous (1.73) for the whole investigated structure.

18. J. Virieux, *Geophysics* **51**, 889 (1986). The equations of motion for elastic velocities and stresses were approximated by FD formulas based on a staggered-grid scheme for space and time steps. Earth's surface was approximated by a discontinuous topography above which stress was assumed to be zero. In our FD simulations, a discretized 2D medium with a grid of points equally spaced in the *x* and *z* directions ($\Delta x = \Delta z = 50$ m) was used. At each grid point, *P*- and *S*-wave velocity were assigned according to the velocity model used for ray-tracing analysis except that an average velocity profile was used to simulate the velocity variation in shallow volcanic sediments.
19. A. R. Sanford, O. Altepkin, T. R. Toppozada, *Bull. Seismol. Soc. Am.* **63**, 2021 (1973); M. Mizoue, I. Nakamura, T. Yokota, *Bull. Earthquake Res. Inst.* **57**, 653 (1982); S. Matsumoto and A. Hasegawa, *J. Geophys. Res.* **101**, 3067 (1996).
20. E. N. Bessonova, V. M. Fishman, V. Z. Ryaboy, G. A. Sitnikova, *Geophys. J. R. Astron. Soc.* **36**, 377 (1974).
21. C. H. Thurber, *J. Geophys. Res.* **88**, 8226 (1983).
22. R. De Matteis, A. Zollo, J. Virieux, in preparation; A. Zollo, *et al.*, *Ann. Geofis.*, in press; H. Le Meur, A. Zollo, G. De Natale, J. Virieux, in preparation.
23. We acknowledge two anonymous reviewers for their helpful and critical comments on the manuscript. The seismic tomography of Vesuvius is supported by the Gruppo Nazionale di Vulcanologia, CNR, Italy. This research was cosponsored by the Istituto Italiano di Studi Filosofici, Naples, Conferenza Permanente dei Rettori (Progetto Galileo), and the French embassy in Italy. It was also financially supported through the Ministero per l'Università e la Ricerca Scientifica e Tecnologica (40%) (P.G.).

24 April 1996; accepted 23 July 1996

Presynaptic Calcium Current Modulation by a Metabotropic Glutamate Receptor

Tomoyuki Takahashi,* Ian D. Forsythe, Tetsuhiro Tsujimoto, Margaret Barnes-Davies, Kayoko Onodera

Metabotropic glutamate receptors (mGluRs) regulate transmitter release at mammalian central synapses. However, because of the difficulty of recording from mammalian presynaptic terminals, the mechanism underlying mGluR-mediated presynaptic inhibition is not known. Here, simultaneous recordings from a giant presynaptic terminal, the calyx of Held, and its postsynaptic target in the medial nucleus of the trapezoid body were obtained in rat brainstem slices. Agonists of mGluRs suppressed a high voltage-activated P/Q-type calcium conductance in the presynaptic terminal, thereby inhibiting transmitter release at this glutamatergic synapse. Because several forms of presynaptic modulation and plasticity are mediated by mGluRs, this identification of a target ion channel is a first step toward elucidation of their molecular mechanism.

Presynaptic inhibition mediated by the mGluR family (1) has been implicated in autoreceptor inhibition at mammalian glu-

tamatergic synapses (2) and in lateral inhibition at dendrodendritic synapses (3), and more generally in reducing transmitter depletion (4). Presynaptic mGluRs are also crucially involved in the induction of long-term depression at hippocampal mossy fiber-CA3 synapses (5). Pharmacological studies with type-specific agonists indicate that mGluR subtypes 2 and 3 (3, 5) or subtypes 4, 6, 7, and 8 (2, 6) may mediate presynaptic inhibition. Several potential

T. Takahashi, T. Tsujimoto, K. Onodera, Department of Neurophysiology, Institute for Brain Research, Faculty of Medicine, University of Tokyo, Tokyo 113, Japan.
I. D. Forsythe and M. Barnes-Davies, Ion Channel Group, Department of Cell Physiology and Pharmacology, University of Leicester, Post Office Box 138, Leicester LE1 9HN, UK.

*To whom correspondence should be addressed. E-mail: ttakahas-ky@umin.u-tokyo.ac.jp

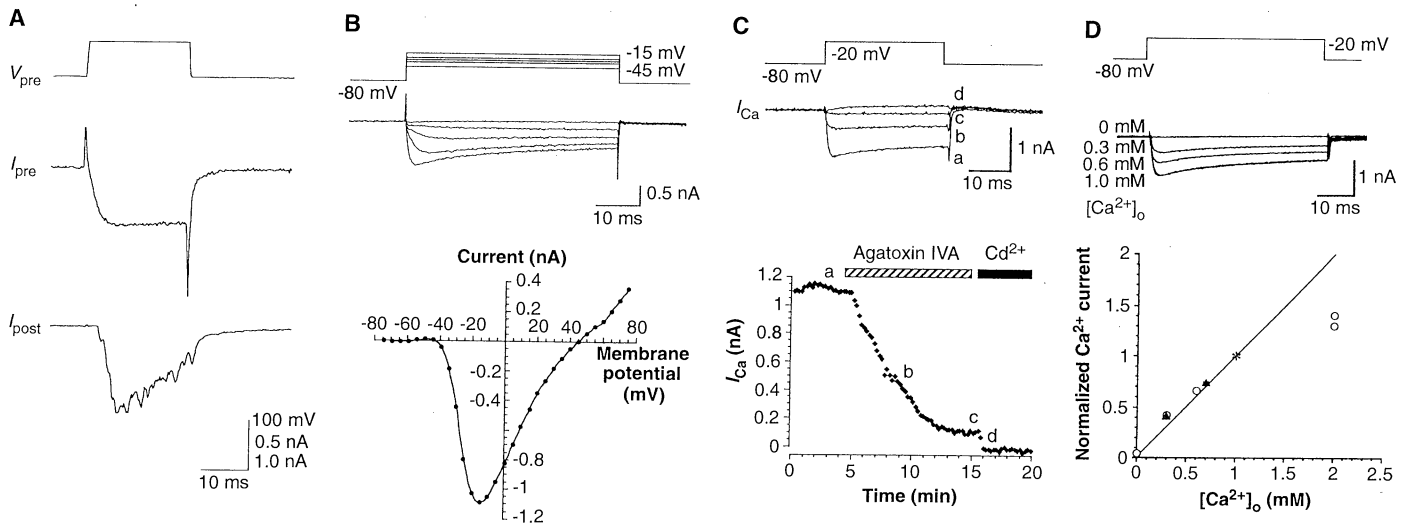


Fig. 1. (A) Simultaneous whole-cell recording from the calyx of Held and its postsynaptic target, both held at -70 mV under voltage clamp. Presynaptic Ca^{2+} currents (middle record) that were evoked by a depolarizing command pulse (top) produced a sustained EPSC (bottom). (B) The Ca^{2+} current-voltage relation. Records (top) are Ca^{2+} currents evoked by depolarization from -80 mV to -45 to -15 mV. $[\text{Ca}^{2+}]_o$ was 1 mM. (C) Block of the presynaptic Ca^{2+} current by ω -agatoxin IVA [200 nM with cytochrome c (1 mg/ml)]. The residual current (8%) was abolished by 100 μM Cd^{2+} . Striped and solid bars indicate the periods of

agatoxin and Cd^{2+} exposure, respectively. Records (top) show superimposed Ca^{2+} currents for the different conditions (a through d). (D) Relation between Ca^{2+} current amplitude and $[\text{Ca}^{2+}]_o$. Records (top) show Ca^{2+} currents evoked by a 50 -ms pulse from -80 to -20 mV (\circ) or a 1 -ms pulse from -70 to $+30$ mV (\blacktriangle). The peak amplitude of Ca^{2+} currents was normalized to that at 1 mM ($*$). Except for 2 mM $[\text{Ca}^{2+}]_o$ (two calyces), data represent means and SEMs (merged in symbols) derived from four calyces each (for both long- and short-pulse protocols). The solid line indicates a one-to-one linear relation.

mechanisms have been suggested to account for this mGluR effect; these include suppression of a presynaptic calcium conductance (7), augmentation of a potassium conductance (4, 8, 9), or inhibition of the exocytotic machinery downstream of calcium influx (10, 11). Any investigation of these possibilities requires direct access to both the presynaptic and postsynaptic sites of a mammalian synapse, as has previously been conducted at invertebrate synapses (12) and chick autonomic ganglia (13).

We made simultaneous whole-cell recordings of the presynaptic Ca^{2+} current and the excitatory postsynaptic current (EPSC) using a rat brainstem slice preparation containing a giant synapse called the calyx of Held (14, 15). This glutamatergic synapse forms on the cell bodies of neurons in the medial nucleus of the trapezoid body (MNTB), and mGluR agonists are known to inhibit transmitter release at this site (10). Transmitter release was induced by voltage-dependent Ca^{2+} currents elicited in the presynaptic terminal under voltage clamp (16).

When presynaptic Ca^{2+} currents were evoked by a long depolarizing pulse, sustained EPSCs resulting from asynchronous transmitter release were recorded from a postsynaptic neuron (Fig. 1A). Short Ca^{2+} currents produced fast EPSCs (see below) that were comparable in time course with those evoked by nerve stimulation (10). The presynaptic Ca^{2+} current was activated on depolarization positive to -40 mV and

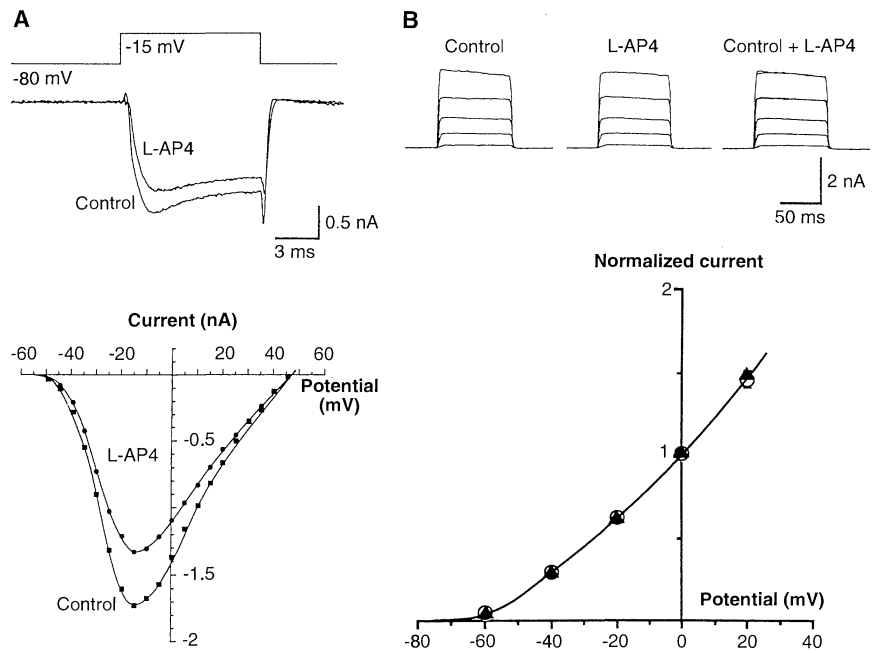


Fig. 2. L-AP4 suppressed the presynaptic Ca^{2+} current but had no effect on the potassium current. (A) Suppression of the presynaptic Ca^{2+} current by L-AP4 (100 μM , applied from a local puffer pipette). Upper panel: Ca^{2+} currents before and after L-AP4 application, superimposed. Lower panel: The Ca^{2+} current-voltage relation before and after L-AP4 application. $[\text{Ca}^{2+}]_o$ was 1 mM. (B) L-AP4 had no effect on the presynaptic potassium current. Upper panel: The outward potassium currents were evoked by 20 -mV incremental depolarizing steps from -80 mV holding potential in the presence of TTX (1 μM). Potassium currents before (left) and after L-AP4 application (50 μM , center) were completely superimposed when overlaid (right). Lower panel: The potassium current-voltage relations before (\circ) and after L-AP4 application (\blacktriangle) were indistinguishable. Means and SEMs derived from four calyces are normalized to those at 0 mV; line drawn by eye.

reached a peak at -20 to -10 mV (Fig. 1B), which indicated that it is a high voltage-activated (HVA) type. The Ca^{2+} current

was largely blocked by the P-type Ca^{2+} channel blocker ω -agatoxin IVA (200 nM, Fig. 1C); it was depressed by $96 \pm 1.7\%$

(mean \pm SEM, $n = 7$). A small residual component was abolished by 100 μM Cd^{2+} . As at other central synapses (17), the L-type Ca^{2+} channel blocker nifedipine (or nimodipine; 10 μM) had no effect ($n = 3$). Unexpectedly, however, the N-type Ca^{2+} channel blocker ω -conotoxin GVIA (2 μM) also had little or no effect on the Ca^{2+} current at this synapse ($n = 5$) (18). As at the squid giant synapse (19), the amplitude of the presynaptic Ca^{2+} current decreased with reduced external Ca^{2+} concentration ($[\text{Ca}^{2+}]_o$) (Fig. 1D) or with increased $[\text{Mg}^{2+}]_o$ (18). The relation between the peak amplitude of the Ca^{2+} current and $[\text{Ca}^{2+}]_o$ was approximately linear below 1 mM (Fig. 1D).

To clarify the mechanism by which mGluR agonists depress transmitter release, we first examined whether they might modulate the presynaptic Ca^{2+} current. When L-2-amino-4-phosphonobutyrate (L-AP4, 50 to 100 μM), an agonist of mGluR subtypes 4, 6, 7, and 8, was added to the bathing solution, the presynaptic Ca^{2+} current was clearly suppressed, particularly at an early phase around the peak (Figs. 2A and 3A) by $25.2 \pm 4.2\%$ ($n = 21$ calyces, evoked by step depolarizations 1 to 50 ms). This effect was reversible after washout of the agonist (Fig. 3B). A similar effect was observed for a broader-spectrum mGluR agonist, (1S,3S)-1-aminocyclopentane-1,3-dicarboxylic acid

(1S,3S-ACPD, 100 μM), whereas (2S,1'R,2'R,3'R)-2-(2,3-dicarboxycyclopropyl)glycine (DCG-IV, 3 μM) (3), a specific agonist of mGluR subtypes 2 and 3, had no effect ($n = 3$). Thus, one or more of mGluR subtypes 4, 6, 7, and 8 may be involved in this effect. This mGluR-mediated depression was not accompanied by a shift in the voltage dependence of the Ca^{2+} current, as shown by a constant current-voltage relation before and after L-AP4 application (Fig. 2A).

We next examined whether L-AP4 might act by potentiation of a presynaptic potassium current. An outward potassium current was evoked by depolarization of a calyx voltage-clamped at -80 mV in the presence of tetrodotoxin (TTX, 1 μM) (14). The potassium current was activated on depolarization positive to -60 mV and its magnitude increased steeply on further depolarization (Fig. 2B). In all four calyces examined, L-AP4 (50 μM) had no effect on the potassium current (Fig. 2B).

Paired recordings from a presynaptic terminal and its postsynaptic target showed a concurrent suppression of presynaptic Ca^{2+} current and EPSC during L-AP4 application (Fig. 3A). The inhibition was $24.3 \pm 6.2\%$ for the Ca^{2+} currents (evoked by a 1-ms pulse) and $40.0 \pm 4.7\%$ for the EPSCs ($n = 9$ pairs). To determine whether the suppression of Ca^{2+} current could account

for the reduction in the EPSC, we examined the relation between the Ca^{2+} current amplitude and the respective EPSCs in the same recording, first during reduction of $[\text{Ca}^{2+}]_o$ and subsequently during application of L-AP4. When $[\text{Ca}^{2+}]_o$ was reduced by replacement with Mg^{2+} , the presynaptic Ca^{2+} currents and EPSCs were diminished in parallel (Fig. 3B). When the Ca^{2+} current-EPSC relations were plotted from data points derived from the reduction of $[\text{Ca}^{2+}]_o$ and application of L-AP4, a similar slope was observed (Fig. 3C). The mean slopes of the regression lines were 2.10 ± 0.37 and 1.93 ± 0.30 , respectively, for the $[\text{Ca}^{2+}]_o$ reduction data and the L-AP4 application data ($n = 6$ pairs, not significantly different by Student's t test). Thus, presynaptic inhibition by mGluR is mediated by suppression of the presynaptic Ca^{2+} conductance at the rat calyx-MNTB synapse.

We investigated the ionic basis of mGluR-mediated presynaptic inhibition by making patch-clamp recordings from both the presynaptic and postsynaptic sites of an identified synapse. The presynaptic Ca^{2+} current at the calyx of Held was of the HVA type and was mediated predominantly by the P/Q-type Ca^{2+} channels. This presynaptic Ca^{2+} current was clearly suppressed by the mGluR agonists. Thus, our finding corresponds to previous results concerning somatic Ca^{2+} currents that are suppressed by a variety of receptor agonists (20), including those of mGluRs (7). Recent studies using Ca^{2+} -sensitive dyes indicate that presynaptic Ca^{2+} entry into a population of nerve terminals can be suppressed by agonists of mGluRs (9) and other receptors (21). Suppression of presynaptic Ca^{2+} entry can be the result of either suppression of presynaptic Ca^{2+} channels or augmentation of potassium channels (4, 8, 9, 22). At the calyx-MNTB synapse, L-AP4 had no effect on the voltage-dependent potassium currents in the preterminal. Thus, potassium channels do not appear to be involved in the presynaptic mGluR modulation at this synapse. Our results also emphasize the need for cautious interpretation of the results from indirect methods when studying presynaptic mechanisms since previous work on the EPSCs at the calyx-MNTB synapse suggested that, on the basis of paired-pulse experiments, mGluRs had no effect on the presynaptic Ca^{2+} current (10).

To examine whether mGluRs may additionally modulate the exocytotic machinery downstream of Ca^{2+} entry, we compared the Ca^{2+} current-EPSC relation under two conditions: reduction of $[\text{Ca}^{2+}]_o$ and application of L-AP4. The close agreement of these input-output relations suggests that presynaptic inhibition by mGluRs is largely

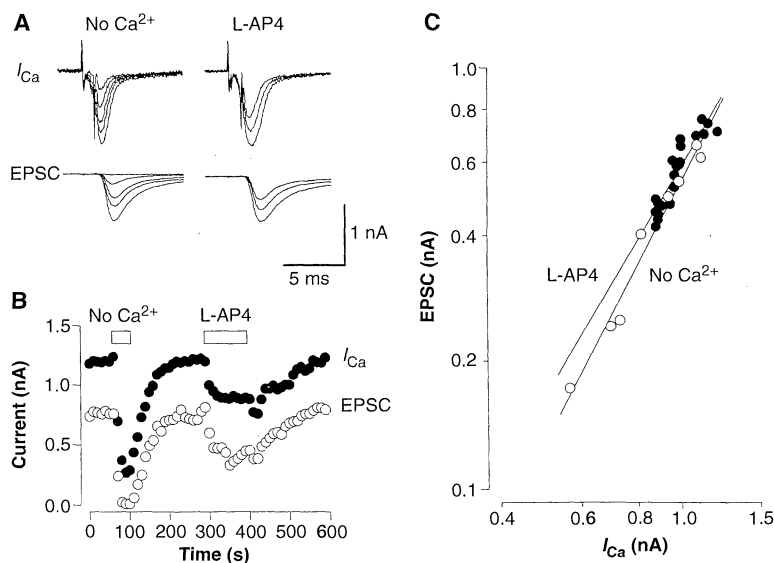


Fig. 3. Suppression of presynaptic Ca^{2+} currents and EPSCs by L-AP4 and reduced $[\text{Ca}^{2+}]_o$ in a paired recording from a calyx-MNTB synapse. **(A)** Presynaptic Ca^{2+} currents (evoked by a 1-ms pulse from -70 to $+30$ mV) and the resultant EPSCs (at -70 mV) after 2 mM $[\text{Ca}^{2+}]_o$ was replaced by 5 mM Mg^{2+} (left) or after L-AP4 application (50 μM , right), superimposed. **(B)** Time plots of presynaptic Ca^{2+} currents and EPSCs. Open bars indicate the period of $[\text{Ca}^{2+}]_o$ reduction and L-AP4 application, respectively. **(C)** Peak amplitude of the presynaptic Ca^{2+} current plotted against the amplitude of EPSCs in double logarithmic coordinates. \circ , Data points obtained from the period of $[\text{Ca}^{2+}]_o$ reduction; \bullet , data points from the period of L-AP4 application. Data points include those at both onset and recovery but exclude those at the baseline ($>10\%$ change of EPSC amplitude) and peak ($>90\%$). The linear regression slopes for $[\text{Ca}^{2+}]_o$ reduction and L-AP4 application were 2.06 and 1.82, respectively, in this experiment.

caused by the suppression of presynaptic Ca^{2+} current at the calyx-MNTB synapse. Direct modulation of the exocytotic machinery by mGluRs has been suggested from the reduced frequency of spontaneous miniature synaptic current by mGluR agonists (11); however, miniature frequency does not always display a direct relation to evoked transmitter release during presynaptic modulation (23). Although the possibility that washout may influence mechanisms downstream of Ca^{2+} currents cannot be excluded from this whole-cell study, our results strongly suggest that presynaptic Ca^{2+} channels are the main target for the mGluR-mediated presynaptic inhibition at the calyx of Held. Because P/Q-type Ca^{2+} channels mediate fast synaptic transmission at a variety of central synapses (17) and mGluRs are widely distributed in central presynaptic terminals (24), modification of the P/Q-type calcium channel may be a general mechanism underlying presynaptic modulation by mGluRs.

REFERENCES AND NOTES

1. S. Nakanishi, *Neuron* **13**, 1031 (1994); D. D. Schoepp and P. J. Conn, *Trends Pharmacol. Sci.* **14**, 13 (1993).
2. I. D. Forsythe and J. D. Clements, *J. Physiol. (London)* **429**, 1 (1990); A. Baskys and R. C. Malenka, *ibid.* **444**, 687 (1991).
3. Y. Hayashi et al., *Nature* **366**, 687 (1993).
4. F. Sladeczek, A. Momiyama, T. Takahashi, *Proc. R. Soc. London Ser. B* **253**, 297 (1993).
5. K. Kobayashi, T. Manabe, T. Takahashi, *Science* **273**, 648 (1996); M. Yokoi et al., *ibid.*, p. 645.
6. T. Takahashi, A. Momiyama, S. G. Cull-Candy, *J. Physiol. (London)* **446**, 549P (1992).
7. K. J. Swartz and B. P. Bean, *J. Neurosci.* **12**, 4358 (1992); Y. Sahara and G. L. Westbrook, *ibid.* **13**, 3041 (1993).
8. D. M. Lovinger, E. Tyler, S. Fidler, A. Merritt, *J. Neurophysiol.* **69**, 1236 (1993).
9. M. Yoshino and H. Kamiya, *Brain Res.* **695**, 179 (1995).
10. M. Barnes-Davies and I. D. Forsythe, *J. Physiol. (London)* **488**, 387 (1995).
11. J.-C. Poncelet, H. Shinozaki, R. Miles, *ibid.* **485**, 121 (1995); I. Llano and A. Marty, *ibid.* **486**, 163 (1995).
12. B. Katz and R. Miledi, *ibid.* **192**, 407 (1967); N. Kawai and A. Niwa, *ibid.* **305**, 73 (1980).
13. A. R. Martin and G. Pilar, *ibid.* **168**, 443 (1963); E. F. Stanley and G. Goping, *J. Neurosci.* **11**, 985 (1991); H. yawo and A. Momiyama, *J. Physiol. (London)* **460**, 153 (1993).
14. I. D. Forsythe, *J. Physiol. (London)* **479**, 381 (1994).
15. J. G. G. Borst, F. Helmchen, B. Sakmann, *ibid.* **489**, 825 (1995).
16. Transverse slices (150 μ m thick) of superior olivary complex were prepared from Wistar or Lister Hooded rats killed by decapitation at the age of 8 to 18 days [F. A. Edwards, A. Konnerth, B. Sakmann, T. Takahashi, *Pfluegers Arch.* **414**, 600 (1989); I. D. Forsythe and M. Barnes-Davies, *Proc. R. Soc. London Ser. B* **251**, 143 (1993)]. The MNTB neurons and calyces were viewed with an upright microscope with a 63 \times objective (Zeiss) through a charge-coupled device camera. Each slice was superfused with artificial cerebrospinal fluid (aCSF) containing 120 mM NaCl, 2.5 mM KCl, 26 mM NaHCO₃, 1.25 mM Na₂HPO₄, 2 mM CaCl₂, 1 mM MgCl₂, 3 mM myo-inositol, 2 mM sodium pyruvate, 0.5 mM ascorbic acid, and 4 mM lactic acid (pH 7.4 with 5% CO₂ and 95% O₂); when measuring Ca²⁺ currents, 10 mM tetraethylammonium (TEA) chloride, 1 μ M TTX, 10

μ M bicuculline, and 0.5 μ M strychnine were also included. The postsynaptic patch pipette contained 97.5 mM potassium gluconate, 32.5 mM KCl, 10 mM Hepes, 5 mM EGTA, and 1.0 mM MgCl₂ (pH 7.3). *N*-(2,6-diethylphenylcarbonylmethyl)-triethylammonium bromide (QX314, 5 mM) was routinely included in the postsynaptic pipette solution to suppress action potential generation. The presynaptic pipette solution contained 110 mM CsCl, 40 mM Hepes, 0.5 mM EGTA, 1 mM MgCl₂, 2 mM adenosine triphosphate (ATP), 0.5 mM guanosine triphosphate (GTP), 12 mM phosphocreatinine, and 10 mM TEA (pH adjusted to 7.4 with CsOH); 10 mM cesium glutamate was added in replacement with equimolar CsCl in some experiments. For recording presynaptic potassium currents, TEA was omitted from aCSF solution and the pipette was filled with the postsynaptic solution including ATP, GTP, and phosphocreatinine at the above concentrations. Recordings were made at room temperature (22° to 25°C). The liquid junction potential between the pipette and aCSF (+2 mV) was not corrected. The electrode resistances were 5 to 10 megohms for the postsynaptic pipette and 7 to 12 megohms for the presynaptic pipette. Series resistances (10 to 30 megohms) were compensated by 50 to 90%. Records were low-pass filtered at 2 to 10 kHz and digitized at 5 to 27 kHz by means of a CED 1401 interface (Cambridge Electronic Design). Leak currents were subtracted for presynaptic currents by a P/N protocol.

17. T. Takahashi and A. Momiyama, *Nature* **366**, 156 (1993); D. B. Wheeler, A. Randall, R. W. Tsien, *Science* **264**, 107 (1994); S. Sivaramakrishnan and G. Laurent, *J. Neurosci.* **15**, 6576 (1995).
18. T. Takahashi, T. Tsujimoto, K. Onodera, I. D. Forsythe, M. Barnes-Davies, data not shown.
19. G. J. Augustine and M. P. Charlton, *J. Physiol. (London)* **381**, 619 (1986).
20. R. Anwyl, *Brain Res. Rev.* **16**, 265 (1991).
21. L.-G. Wu and P. Saggau, *Neuron* **12**, 1139 (1994); *J. Physiol. (London)* **485**, 649 (1995); J. S. Dittman and W. G. Regehr, *J. Neurosci.* **16**, 1623 (1996).
22. S. A. Siegelbaum, J. S. Carmado, E. R. Kandel, *Nature* **299**, 413 (1982).
23. W.-m. Fu and M.-m. Poo, *Neuron* **6**, 837 (1991); Y. Hori, K. Endo, T. Takahashi, *J. Physiol. (London)* **492**, 867 (1996).
24. H. Ohishi et al., *Neuron* **13**, 55 (1994); *J. Comp. Neurol.* **360**, 555 (1995); R. Shigemoto et al., *Nature* **381**, 523 (1996).
25. We thank M. Farrant, T. Manabe, and K. Kobayashi for comments on early drafts and Y. Ofune for DCG-IV. Supported by a grant-in-aid for scientific research from the Ministry of Education of Japan, the Wellcome Trust, and a travel grant from Yamada Science Foundation. I.D.F. is a Wellcome Senior Research Fellow in Basic Biomedical Sciences.

1 May 1996; accepted 13 August 1996

Identification of an Asymmetrically Localized Sensor Histidine Kinase Responsible for Temporally and Spatially Regulated Transcription

James A. Wingrove and James W. Gober*

Caulobacter crescentus undergoes asymmetric cell division, resulting in a stalked cell and a motile swarmer cell. The genes encoding external components of the flagellum are expressed in the swarmer compartment of the predivisional cell through the localized activation of the transcription factor FliB. The mechanisms responsible for the temporal and spatial activation of FliB were determined through identification of FliE, a histidine kinase required for FliB activity. FliE is asymmetrically distributed in the predivisional cell. It is located at the pole of the stalked compartment and at the site of cell division in the swarmer compartment. These findings suggest that FliE and FliB are activated in response to a morphological change in the cell resulting from cell division events.

The generation of asymmetry is a critical event in the developmental programs of many organisms, including bacteria, yeast, and multicellular organisms (1). Asymmetrical cell divisions can arise either as a consequence of external influences on the cell or as a result of intrinsic signals built into the architecture of the cell. An intrinsically governed asymmetric cell division in the bacterium *Caulobacter crescentus* produces two morphologically distinct progeny cells: a stalked cell and a motile swarmer cell with a single polar flagellum (2). Several genes encoding external flagellar components are preferentially transcribed in the

swarmer compartment of the late predivisional cell (3). Compartmentalized expression of late flagellar genes is attributable to the swarmer pole-specific activation of the transcriptional regulator protein FliB (4). Activated FliB also functions as a swarmer pole-specific repressor of the early *fliF* promoter (5, 6). FliB is homologous to a large family of two-component response regulators (6), members of which are active when phosphorylated on a conserved aspartate residue (7). The activating phosphate is typically obtained from sensor histidine kinases that are capable of undergoing autophosphorylation, often in response to an external environmental cue. Once phosphorylated, histidine kinases serve as phosphodonors for their cognate response regulators.

A potential candidate histidine kinase

Department of Chemistry and Biochemistry and the Molecular Biology Institute, University of California, Los Angeles, CA 90095-1569, USA.

*To whom correspondence should be addressed.